Published in final edited form as:
J Comp Neurol. 2009 August 1; 515(4): 441–453. doi:10.1002/cne.22088.

Drosophila Serotonergic Varicosities Are Not Distributed in a Regular Manner

JOHN CHEN[1,2] and **BARRY G. CONDRON**[1,*]

[1] Department of Biology, University of Virginia, Charlottesville, Virginia 22903

[2] University of Virginia Medical Scientist Training Program, Charlottesville, Virginia 22903

Abstract

Neurons of the brain form complex tree-like structures that are critical for function. Here we examine the spatial pattern of serotonergic varicosities, the synaptic sites of serotonin release in the central nervous system (CNS). These varicosities are thought to form largely nonjunctional-type connections that partition in a grid-like manner in order to distribute evenly the neuromodulatory neurotransmitter serotonin. We describe the neuropil distribution of serotonergic varicosities in the brain and ventral nerve cord (VNC) of the larval *Drosophila* CNS. In the brain, we find evidence for avoidance between varicosities at distances lower than 1.75 μm. However, in the VNC, we find a clustered distribution. A similar clustered pattern is found in the *Xenopus* brain. This pattern produces many varicosities that are clustered together but also includes some varicosities that are very isolated. These isolated varicosities are not found along particular topological sections of the neurite tree or in particular locations in the CNS. In addition, the pattern breaks down when serotonergic branches of adjacent segments invade each other's territory. The pattern is similar to those described by a power law.

Indexing terms

serotonin; *Drosophila*; varicosities; Levy pattern; heavy-tailed distribution

Serotonin is a monoamine neurotransmitter that is released from serotonergic neurons in the central nervous system (CNS). There, serotonin plays a role in modulating most neuronal circuits, and therefore has influences on many human behaviors (Jacobs and Azmitia, 1992). Altered serotonin levels and wiring are thought to play key roles in the etiology of many neuropsychiatric illnesses. Although serotonin is a key player in many human behaviors and diseases, little is known about the branching and patterning of the serotonergic system. Whereas some parts of the brain are thought to use predominantly synaptic transmission of serotonin, most regions are thought to communicate with their targets primarily through volumetric transmission, whereby serotonin is released from nonjunctional presynaptic varicosities (Chazal and Ralston, 1987; Moukhles et al., 1997; Bunin and Wightman, 1998; De-Miguel and Trueta, 2005). Volumetric transmission is used by several other neuromodulatory neurotransmitter systems, including the dopaminergic system (Bunin and Wightman, 1999).

Serotonin is believed to diffuse 5 μm from a presynaptic varicosity release site and still maintain a functional concentration (Bunin and Wightman, 1998). On the basis of serotonin receptor distribution, most areas of the brain are thought to require serotonin modulation. Serotonergic varicosities are therefore predicted to be distributed in a somewhat regular array so as to ensure

*Correspondence to: Barry G. Condron, Department of Biology, University of Virginia, Gilmer Hall 071, Box 400328, Charlottesville, VA 22903. condron@virginia.edu.

that serotonin can diffuse evenly to all of its targets (Bunin and Wightman, 1998). Previous spatial point analysis of the distribution of nonserotonergic synapses has provided support for the idea that presynaptic boutons are regularly spaced (Meinertzhagen et al., 1998). However, the actual spatial patterning of serotonergic innervation remains unknown.

Many systems in nature face a similar problem of space filling, including the human bronchial and arterial system. Both the bronchial airways and blood vessels in the arterial system must be efficiently distributed in order to achieve proper gas and nutrient exchange, respectively. Both systems begin with stereotypical branching patterns that break down into a fractal structure after several generations of branching. Although a regular organization would seem to provide the most efficient means of space filling, the majority of their branches are dominated by a clustered scale-free pattern, also referred to as a fractal (Mandelbrot, 1977; McNamee, 1991; Bassingthwaighte et al., 1994). In order to better understand the patterning of the serotonergic system, we have utilized the *Drosophila* serotonergic system because of its simplicity and genetic amenability. By using a variety of spatial analyses, we examine varicosity distribution in the brain and the ventral nerve cord (VNC). In one part of the brain, we find a partially regular pattern. However, in the VNC, we find a distribution that is clustered over a broad scale. In addition, whereas each branched structure within a segment is clustered, branches from adjacent segments break down the overall clustering, and the pattern becomes more random.

MATERIALS AND METHODS

Animals

Drosophila stocks (*UAS-hb*, *UAS-mCD8-GFP*, *UAS-syntaxin-GFP*, *UAS-robo2*, *eg-GAL4*, and *ddc-GAL4*) were obtained from the Bloomington stock center.

For green fluorescent protein (GFP) clonal analysis, we used the *hs-FLP;UASy+cd8-GFP*, kindly provided by Barry Dickson (Institute of Molecular Biotechnology, Vienna). Cell ablation was achieved by targeted expression of *UAS-rpr-hid*, kindly provided by Paul Taghert (Washington University School of Medicine, St. Louis, MO). *Tph-GAL4* was a gift from by Jaeseob Kim (Korea Advanced Institute of Science and Technology, Daejeon, Korea). *Xenopus* samples were obtained from Dr. Lance Davidson (University of Virginia, Charlottesville, VA).

Dissection and immunohistochemistry

Drosophila VNCs and *Xenopus* brains were dissected in Schneider's insect media and fixed for 1 hour in 4% paraformaldehyde. Samples were incubated in phosphate-buffered saline plus 0.1% Triton-X-100 (PBT) overnight at room temperature with primary antibodies, anti-serotonin (rabbit polyclonal, ImmunoStar, Hudson, WI, #20080) at a dilution of 1:1,000. This rabbit anti-serotonin antibody was generated against serotonin coupled to bovine serum albumin with paraformaldehyde. The antibody stains the same pattern as an anti-serotonin monoclonal but does not stain fly mutants unable to synthesize serotonin (Vallés and White, 1986). GFP signal was enhanced by staining with anti-GFP (chicken polyclonal, Abcam, Cambridge, MA, #ab13970) at a dilution of 1:1,000. This chicken anti-GFP antibody was prepared against recombinant full-length jellyfish *Aequorea victoria* GFP. Western blot analysis of transgenic mouse spinal cords shows that the chicken anti-GFP recognizes a band of the correct molecular weight and only in animals expressing the protein (manufacturer's technical information). In addition, histochemical staining is seen only in cells expressing GFP. In *Drosophila*, staining is seen only in those cells expressing GFP under GAL4 control. No staining is seen when GFP is not expressed transgenically in the VNC.

Fasciclin II bundles were stained with a mouse monoclonal antibody, mAb FasII (Developmental Studies Hybridoma Bank, Ames, IA, #1D4) at a dilution of 1:100. This mouse monoclonal antibody was prepared against a bacterially expressed fusion peptide containing the intracellular C-terminal 103 amino acids of the PEST transmembrane form of FasII (Helt, 1997). 1D4 stains the same *Drosophila* CNS pattern as two other independently prepared FasII antibodies, each using different immunogens to 1D4: a rat anti-FasII serum antibody prepared by using an internal portion of the protein (Grenningloh et al., 1991), and an anti-extracellular domain peptide-derived rabbit antiserum (Mathew et al., 2003). The rat anti-FasII serum antibody-staining pattern, which is the same as that of 1D4, is completely lost in a fasII null mutant. The rat FasII serum, like 1D4 (Mathew et al., 2003), recognizes a single 97-kDa protein species of the correct estimated size on Western blots and this is lost in FasII null mutants (Grenningloh et al., 1991).

AlexaFluor goat anti-rabbit, goat anti-chicken, and goat anti-mouse secondaries (Molecular Probes, Eugene, OR) were used at 1:1,000 in PBT overnight at room temperature. No secondary staining was seen in *Drosophila* tissue not preincubated with primary antibody. Samples were mounted on slides in 90% glycerol/2.5% 1,4-diazabicyclo[2.2.2]octane (DABCO).

Analysis

Imaging was done with a Nikon eclipse E800 confocal microscope (100×) and recorded with Perkin-Elmer (Oak Brook, IL) software. Confocal stacks were taken from the top of the neuropil through the cell bodies at the abdominal region of the ventral nerve cords. For *Xenopus* brains, the diencephalon was imaged. Image stacks that were obtained from the confocal microscope were imported directly into Volocity 3.7 (Improvision, Inc., a PerkinElmer Company, Waltham, MA). Images were cropped and auto-leveled in Volocity and panels were then imported into Microsoft PowerPoint for the creation of the figures (Sykes and Condron, 2005; Chen and Condron, 2008). For classification, the intensity distribution was bounded at both minimum and maximum, with options of noise reduction, object separation, and size threshold of 0.2 and 8 μm^3. Classification provided quantification and the x,y,z coordinates of varicosities. Voronoi volumes surrounding varicosities were calculated from the x,y,z coordinates by using custom-designed Matlab, Excel, and Java software, which all give the same results (Condron, 2008). The Voronoi volumes were binned in 5-μm^3 volume increments for histogram analysis. Lacunarity analysis was adopted and modified from Plotnick et al. (1996). Branch reconstruction was performed as described (Chen and Condron, 2008). Student's t-test was performed with Instat software.

RESULTS

Varicosity spacing in various parts of the fly CNS

Serotonergic varicosities are found in all or most parts of the metazoan neuropil and are thought to distribute evenly in the CNS, perhaps by a self-avoidance mechanism. In *Drosophila*, serotonergic varicosities can be visualized by staining for serotonin and defined morphologically as structures 0.2–8 μm^3 (Sykes and Condron, 2005). By visual inspection of the *Drosophila* third-instar larval CNS, the region with the most intense and densest varicosity staining is the ventrolateral protocerebrum (VLP) in the central brain (Fig. 1A,B). This region was chosen for further analysis because if varicosities exhibit self-avoidance, it would be most expected in this region due to the high density. Varicosities were classified and their Cartesian coordinates obtained as described (Daubert and Condron, 2007; Sykes and Condron, 2005). The varicosity density was 43.1 ± 3.5 per 1,000 μm^3 (n = 6), which is about twice that found in other regions (Sykes and Condron, 2005).

Spatial point analysis can differentiate among random, regular, and clustered distributions of experimental points. Some analytical approaches, such as lacunarity and Voronoi tessellation, can reveal further aspects of the spatial patterning beyond simple classifications of random, regular, and clustered. We first performed radial density analysis, which looks at how the average density changes with distance away from each point (Condron, 2008). For each varicosity, density is measured in a sphere around that varicosity and compared with the overall/bulk sample density. This normalized density, averaged over all varicosities, is plotted against sphere diameter. Although the varicosities located at the periphery will have artificially lower density spheres surrounding them, comparing the spherical densities of randomized points confined to the same boundaries can control for this edge effect (Diggle, 2001). For this control, 100 randomized versions of a single VLP sample were analyzed, and the maximum and minimum of the densities were plotted against increasing sphere diameters (Fig. 1C). This represents the 99% confidence limited region for a random point pattern.

The distribution has higher variance near 1 μm due to the smaller sampling volume and falls off with distance due to boundary effects. Nevertheless, the density is about 1, meaning that density around the points does not change with distance as would be expected for a random distribution. A second simulation used the sample VLP but moved the points onto a 3-μm grid with some noise added. The analysis produces a wavy line as the expanding sampling sphere intersects points on the grid (Fig. 1C). However, the actual analysis of the VLP pattern found in the larval brain demonstrates neither a simple random nor regular pattern. Points show low density up to about 1.75 μm, after which the sample appears random. This was well simulated by a random simulation with 1.75-μm avoidance (often referred to as Poisson with a hardcore; Fig. 1D (Rusakov et al., 1999). From this analysis, we conclude that varicosities are placed in a manner that exhibits avoidance up to 1.75 μm, which results in some degree of local regularity. The average maximum width of a varicosity is about 0.7 μm (Sykes and Condron, 2005). Therefore, the avoidance seen below 1.75 μm cannot be explained by exclusion from the volume of varicosities alone, but rather suggests there may be some other mechanism creating this avoidance.

We next analyzed the serotonergic varicosity pattern found within the fifth abdominal ganglia (A5) of the VNC because it is easily identifiable and neuronal branch architecture has been mapped out (Sykes and Condron, 2005). Anti-serotonin staining of A5 reveals two pairs of serotonergic cell bodies, their commissural axons that extend across the midline, and their projections into the contralateral neuropil, where highly varicose fine axonal processes are found (Fig. 1E). The medial branch pattern was highlighted with syntaxin-GFP (sytGFP), whose expression is driven by tphGAL4 (Chen and Condron, 2008). Non-GFP varicosities derive from A5 lateral serotonergic neurons that do not often express tphGAL4. The position of varicosities is determined by serotonin (5HT) and sytGFP puncta (Fig. 1E,F). Density analysis of the 5HT and sytGFP varicosities reveals a clustered pattern that remains highly clustered over the span of the spherical volumes measured, from 1 to 6 μm (Fig. 1G,H). This clustering could be due to close positioning of varicosities along branches. To test for this, density was measured but now only to varicosities on other branches (thick line in Fig. 1H). A similar clustering was observed, which indicates that clustering is not due to the branch structure. To examine varicosity spacing further, we employed Voronoi tessellation.

The distribution of volumes surrounding serotonergic varicosities has a clustered distribution

Voronoi tessellation involves dividing space among varicosities, with each 1-μm^3 point in space assigned to the nearest varicosity. For comparison, the minimum and maximum distributions of 100 randomized L3F A5 patterns were plotted, indicating the 99% confidence limits for a random pattern (Fig. 2A). The computed 99% confidence limits based on 6 VLP

and 10 L3F A5 distributions were also plotted (Fig. 2A). The density of L3F A5 varicosities is about 20 per 1,000 μm^3. This means that there should be about a 50-μm^3 Voronoi volume surrounding each varicosity if space is partitioned evenly. The random distribution of varicosities of this density would have a broad distribution centered at about 50 μm^3. The VLP is centered below this and has a much tighter distribution, as expected from density analysis.

With the exception of volumes below 10 μm^3 the L3F distribution is a smooth and continuous curve (Fig. 3A) that linearizes on a log-log plot (Fig. 3C) but is less linear when plotted as an exponential distribution on a log-linear plot (Fig. 3B). The distribution does not, by visual inspection, log-normalize (data not shown). The long-tailed distribution seen in L3F A5 is distinct from the distribution seen in VLP and is a random branching pattern (Kolmogorov Smirnov test; $P < 0.0001$). This indicates that the distribution is heavy-tailed clustered and could follow a power law or Weibull statistics. The linearization on a log-log plot is common among spatial distributions that follow a power law. Voronoi volume distributions were measured by the least-squares fit on a log-log plot, r^2, and the clustering was measured by the coefficient of variation of the population (Figs. 2B, 3C). For comparison, a random and a fractal pattern are shown (Fig. 2B). To test the data acquisition method, points were collected either automatically by using the Improvision Volocity classifier (Sykes and Condron, 2005;Daubert and Condron, 2007) or manually (Chen and Condron, 2008) and analyzed by using available software (Condron, 2008). Although variation of r^2 of the automatically obtained points was higher, all of the data sources for L3F A5 indicate high clustering and data that linearize on a log-log plot (Fig. 2B).

Because sample volumes span only 2.5 orders of magnitude, 1–330 μm^3, we cannot truly refer to the Voronoi distribution as scale free or following a power law. The power of the curve, μ, was calculated by linear regression by using six samples of A5 that yielded 1,601 measures and was found to be 1.845. By the maximum-likelihood-estimation (MLE) method, μ was found to be 1.83 for the A5 segment, which falls within the Levy range $1 < \mu \leq 3$ (Edwards et al., 2007) (Table 1). The μ in the lobula, by contrast, with 6 samples and 577 volumes, was found to be 2.92 and 3.08 by linear regression and MLE, respectively. Although the μ for the Voronoi volumes within the A5 segment is indicative of a power law distribution, the Akaike weights suggest that the A5 pattern more closely follows an exponential distribution (0.90) than a power law (0.10; Table 1). For comparison, an idealized fractal pattern was found to follow a power law distribution when its full data set was analyzed by Akaike weights.

Interestingly, if the fractal data set was truncated to volumes less than 300, which is near the cutoff point for the Voronoi volumes in our data due to the limited size of the neuropil, the Akaike weights indicated that the fractal data more closely follows an exponential distribution (Table 1). Another possibility is that the distribution follows Weibull statistics. Modeling with two variables (k, scale factor and λ, shape factor), we find one potential solution that matches our data closely (Fig. 3A,D). Therefore, the A5 pattern is heavy-tailed clustered and could be following either power law or Weibull statistics. Given the small size of the *Drosophila* samples, these distributions may not be distinguishable here.

To determine whether this distribution is *Drosophila*-specific, we looked at serotonin staining in the *Xenopus* diencephalon (Fig. 2C), which has a varicosity density that is similar to that of the *Drosophila* larval A5 region. We found a similar clustered distribution of serotonergic varicosities (Fig. 2D).

Lacunarity analysis suggests that the serotonergic varicosities follow a clustered distribution

To examine the nature of the varicosity distribution further, we performed lacunarity analysis. This is another spatial analysis method that is highly sensitive in differentiating among spatial

distributions, including random, regular, clustered, and fractal (Plotnick et al., 1996). Lacunarity measures the local variability of point density throughout a given sample (1 + variance/mean^2), and is a scale-dependent measure of heterogeneity. The lacunarity of random and regular samples is shown to demonstrate its robustness in differentiating patterns (Fig. 4A). The lacunarity decreases smoothly for a random distribution as the sampling size increases (Fig. 4A). In the regular pattern, peaks can be seen in the lacunarity curve, corresponding to the regular 4-μm grid on which the points are arrayed (Fig. 4A).

In accordance with Voronoi tessellation analysis, lacunarity analysis shows that the serotonergic varicosities within the A5 neuropil are organized in a clustered manner, as revealed by the lacunarity above random values and the linearity of the lacunarity log-log plot (Fig. 4B). This clustered pattern is present for almost the entire size of the neuropil (20–1,200 μm^3). The clustered distribution of serotonergic varicosities is found in every segment within the larval VNC except for the seventh abdominal segment (A7; Fig. 4B and data not shown). Lacunarity analysis demonstrates that the spatial distribution of serotonergic varicosities in A7 of midstage larvae (foraging third instar or L3F) falls within the 99% confidence interval for a random pattern (Fig. 4B).

Random patterns have a characteristic curve to the log-log lacunarity plot, with deviations away from a linear line quantified by r^2 (0.85; Fig. 4C). The lacunarity r^2 for serotonergic varicosities in A7 is 0.89, which is significantly lower than the lacunarity r^2 of A5 (0.93), but still significantly higher than a true random pattern (0.85), and therefore we will refer to this pattern as pseudo-random (Fig. 4C). The differences in pattern can also be seen by comparing the height of the lacunarity curve at 2.5 μm (Fig. 4D). The serotonergic varicosity pattern seen in A5 is more clustered than in both A7 and VLP, as indicated by the higher lacunarity value at 2.5 μm (Fig. 4D). Lacunarity analysis of the other segments within the VNC reveals that all segments, other than A7, are also patterned in a clustered distribution (data not shown).

Within each segment of the VNC, the varicosities originate from numerous serotonergic cells, both from within the segment and from an adjacent segment (Chen and Condron, 2008). In order to examine the varicosity pattern from single serotonergic neurons, the apoptosis genes *reaper* and *hid* (*rpr-hid*) were expressed within the serotonergic neurons early in development to ablate genetically some serotonergic cells and unmask the patterning of single isolated serotonergic neurons (Chen and Condron, 2008). Genetic isolation of single serotonergic neurons revealed that each serotonergic neuron is organized in a clustered distribution (Fig. 4C,D). This pattern was significantly more clustered over a larger scale than the overall pattern created when all serotonergic neurons are intact. Ablation studies suggest that the overlap of multiple scale-free serotonergic projections from neighboring serotonergic segments leads to a degradation in the overall clustered pattern of each segment within the *Drosophila* VNC (Fig. 4C,D). Single isolated A7 serotonergic neurons have branching patterns different from those found in other segments (Chen and Condron, 2008). Lacunarity analysis indicates a pattern that is significantly less clustered than the pattern found in serotonergic neurons from other segments, indicating an intrinsic difference in patterning (Fig. 4C,D). However, like other segments, overlap between serotonergic neurons within the A7 region causes a further degradation in clustered distribution (Fig. 4C,D).

In order to understand further the role of serotonergic overlap in serotonergic patterning, we used a variety of genetic manipulations to increase the amount of overlapping serotonergic innervation. We first overexpressed *hunchback* (*hb*) early in serotonergic development, which is a transcription factor involved in the specification of the medial serotonergic cell (EW1) (Novotny et al., 2002). Early expression of *hb* duplicates, triplicates, or quadruples the number of medial serotonergic cells, with a matching increase in the number of serotonergic branches (Chen and Condron, 2008). This increase in the density of serotonergic branches results in a

significant decrease in the clustering, presumably due to an increase in the amount of serotonergic overlap (Fig. 4B–D).

The presence of a reduction in clustering following an increase in the number of serotonergic branches does not make it possible to distinguish between the contributions of intrasegmentally and intersegmentally overlapping branches. To tease out the differences, we expressed a combination of *rpr-hid* along with *hb* to create isolated triplicates of the medial serotonergic cell. Although there is a large amount of intrasegmental overlap from the triplication of the medial serotonergic cell, the varicosities are patterned in a clustered manner that was indistinguishable from any single isolated serotonergic cell (Fig. 4C,D). This finding suggests that serotonergic innervation originating from within the same segment will organize in this clustered pattern. The decrease in the clustered pattern seen after *hb* expression alone is likely created by an increase in the overlap between segments rather than any change that occurs within a segment.

Varicosity spacing is compatible with a random branching pattern

Most scale-free distributions are thought to arise from interaction among complex entities, but they could also be created by simpler mechanisms. For example, a scale-free distribution of varicosities might result from a smooth varicosity-inducing gradient in the neuropil or varicosity positioning out along a dispersing arbor of neurites. To look for a pattern by position along branches, the large (>100 μm^3 Voronoi volume) varicosities were mapped on six medial cell branch reconstructions (Chen and Condron, 2008). A single dendrogram showing the positions of the large Voronoi volume varicosities is shown as well as a summary of all data (Fig. 5A,B). Large Voronoi volume varicosities are distributed in the same manner as are all other varicosities and are not only found on the ends of branches, as would be expected in a dispersing branched structure. To determine whether large Voronoi volume varicosities are located in a particular part of the CNS, their positions were located in segments counterstained for the axon bundle marker fasciclin II (fasII; Fig. 5C,D). fasII acts as a fiduciary marker for normalizing positions between segments of the CNS. We used the positions of the fasII bundles to register the >100 μm^3 Voronoi volume varicosities in six samples. A summary of the data is shown (Fig. 5C,D). These varicosities appear to be arbitrarily positioned with respect to one another, suggesting that there is no physical constraint creating the clustered distribution. Therefore, the spacing of varicosities seems to follow a nonspecified clustered distribution in space.

We next used computer simulation to model the distribution found in A5 by using different branching parameters. For each model, the same number of points and spatial dimensions of a test A5 branch pattern was used. One hundred simulations of each model were run, and this was used to generate the 99% confidence intervals. For comparison, lacunarity measurements for A5, A5 medial cell triplication (A5 × 3), and a random model are shown (Fig. 5E). For a branched model, a Galton-Watson process was used in which each point has a certain probability of branching (Condron, 2008). In this computer simulation, branching was set at 10%, which produces a dendrogram much like that of real serotonergic neurons (Chen and Condron, 2008). For the first branching model, varicosities are spaced randomly along branches from 0.5 to 8 μm. This produces lacunarity values not significantly different from a random unbranched model.

Next we examined the actual 2D/linear varicosity spacing pattern found along serotonergic branches in the *Drosophila* larvae and found it to be a left-shifted normal pattern (Fig. 5E, right panel). When a similar spacing pattern is incorporated into the branched model, the lacunarity plot is almost indistinguishable from an A5 plot (Fig. 5F). We next extended this model to explain the degradation in the pattern found when the A5 medial cell is triplicated (A5 × 3). By strictly adding more branches to the simulation, there was little degradation in the clustered

pattern (Fig. 5E). However, if avoidance was introduced into the model, there was a significant degradation in the pattern, which suggests that the more random pattern found in A5 × 3 and the degradation in clustering seen in segment overlap are possibly due to this avoidance (Fig. 5E). This indicates that the degradation of the pattern from intersegmental extensions could be due to varicosity avoidance specifically between segments.

DISCUSSION

Clustered patterning of serotonergic varicosities

To modulate a wide range of targets, the serotonergic system sends branches and varicosities throughout the neuropil. Because the majority of neuronal circuits are thought to be modulated by serotonin, the system would be expected to adopt an efficient means of filling the neuropil. We expected the varicosities to be somewhat regularly spaced because this would provide a means of evenly distributing serotonin. However, analysis of the patterning of serotonergic varicosities in the *Drosophila* VNC and the *Xenopus* diencephalon demonstrates that this is not the case. With the use of a variety of spatial analyses, including density distribution, Voronoi tessellation, and lacunarity analyses, we have shown that the serotonergic varicosities in most regions of the *Drosophila* VNC are organized in a clustered distribution

Although we were only able to examine a limited order of magnitude, the varicosity distribution behaves similarly to a fractal pattern. This is supported by lacunarity analysis, whereby the pattern of varicosities within the A5 region of L3F is found to be linear on a log-log lacunarity plot. Further evidence lies within the power, μ, of the Voronoi distribution of varicosities of the A5 region in *Drosophila* larvae. The μ was calculated to be 1.84 by linear regression and MLE, which lies between the expected range for a power law distribution ($1 < \mu \leq 3$; Edwards et al., 2007). Although Akaike weights indicate the distribution better follows an exponential, our analyses of idealized fractal patterns indicate that a large range of values is required for the Akaike weights to favor a power law distribution over an exponential. Because the range of data for Voronoi volumes in our samples is limited at the upper boundary by the size of the neuropil and at the lower boundary by image resolution, we cannot use this test effectively or definitively to state that our pattern follows a power law. The distribution could also follow Weibull statistics. What is needed to distinguish these patterns further are larger tissue samples so that broader scales can be examined. Because the pattern is maintained in vertebrates, an analysis of serotonergic varicosity spacing in a larger brain may resolve this question.

Individual serotonergic neurons were examined with the use of ablation-mediated isolation of individual cells. The pattern from each individual serotonergic neuron was more clustered than the overall serotonergic pattern found within any segment when all serotonergic neurons were intact. The importance of overlap between segments in modifying the clustered pattern was demonstrated by combining genetic duplication and ablation experiments. Increasing the number of serotonergic neurons with early *hb* expression increases the number of serotonergic branches and varicosities, which results in a degradation in the clustered distribution. However, isolated replicated clusters of serotonergic cells have clustered patterns identical to single isolated serotonergic cells. This suggests that serotonergic cells within a segment extend their branches and varicosities in a clustered pattern regardless of the amount of intrasegmental overlap. However, when serotonergic projections overlap from neighboring segments, the interaction between the two independent patterns results in a degradation of the overall clustered pattern.

Utilizing computer simulation of branching, we have demonstrated that the clustered distribution of varicosities can be explained by a random branching pattern. Furthermore, our modeling suggests that increasing the number of branches alone does not alter the pattern, but if avoidance occurs between branches, degradation in the pattern is expected. This may explain

the observed differences in patterning between overlapping intrasegmental and intersegmental serotonergic branches. By extending our findings from our computer simulations, we predict that intersegmental branches display avoidance from one another, resulting in degradation in the pattern between overlapping intersegmental fields of innervation.

Although we have not isolated the factor involved in this potential avoidance, a possible molecule is *Dscam*, which has been shown to mediate repulsion of axons coming from the same cell type between segments (Hughes et al., 2007; Matthews et al., 2007; Soba et al., 2007). Because *Dscam* signaling allows differentiation between self and non-self neuronal identity, it is tempting to suggest that *Dscam* signaling is a potential mechanism involved in the differentiation between intra- and intersegmental varicosity patterning.

In wild-type *Drosophila* larvae, the clustered pattern is found in all scales except at the smallest scale. At the local scale (<20 μm^3), lacunarity analysis and Voronoi tessellation both suggest that the varicosities are distributed in a random-like pattern. Although this may be due to limitations in light microscopy, varicosities at the smallest scale could pattern differently from larger scales. A different spacing rule may apply when varicosities reach within a certain distance threshold of one another. *Dscam* signaling between serotonergic axons in close proximity could be responsible for reducing clustering and generating the more random pattern found at local scales. An alternative is serotonin itself, which has been shown to be able to regulate varicosity density, but it is not clear how this mechanism would differentiate between cells from adjacent segments (Sykes and Condron, 2005).

Why clustered patterning of serotonergic varicosities?

The size of the neuropil within a hemiganglion for an L3F *Drosophila* larvae is approximately 27,000 μm^3 (Sykes and Condron, 2005). It has been estimated that serotonin is able to diffuse 5 μm away from a varicosity release site and still maintain a functional concentration (Bunin and Wightman, 1998). From this assumption, each varicosity creates a spherical diffusion cloud of serotonin that encompasses approximately 500 μm^3. Assuming every part of the neuropil requires serotonin, a regularly distributed serotonergic pattern would need 50–60 varicosities to allow serotonin to diffuse everywhere in the neuropil in each hemisegment of the VNC. However, we find around 500 serotonergic varicosities organized in a clustered manner within the neuropil of each hemisegment, which is 10-fold higher than expected. This would seem to be a waste of resources. In fact, a random placement of varicosities would lead to a more evenly distributed pattern than the clustered pattern that is seen. However, space-filling systems in nature are often organized in a fractal pattern, including the human arterial and bronchial systems, tree branch and root structures, and river networks.

Why would so many systems in nature adopt such a wasteful space-filling method? A number of explanations have been proposed as to why fractal patterns are commonly seen in nature. Perhaps it is easier for nature to achieve a fractal pattern, because fractal patterns can be generated through simple iterative rules. Although somewhat controversial, fractal Levy flight patterns have also been suggested as a means of optimally searching an area, as seen with some predators (Viswanathasn et al., 1999; Bartumeus et al., 2002; Edwards et al., 2007). Therefore, a random Levy-like pattern may be adopted by the branching serotonergic neurons as a means of searching the neuropil in order to obtain adequate innervation. Fractal patterns have also been proposed to provide stability and flexibility in many human physiological systems, including human heartbeat rhythm, gait (Goldberger et al., 2002), tracheobronchial system, arterial and venous system, neuronal firing (Beggs and Plenz, 2003; Plenz and Thiagarajan, 2007), and the brain's functional connectivity (Eguiluz et al., 2005). Therefore, although this clustered distribution of varicosities is not optimal in terms of space filling, it potentially produces a pattern with a broad physiological range that may provide the system with stability.

Taken together, these findings demonstrate an unexpected organization of synapses in the CNS. Furthermore, this pattern presents a clustered distribution that is uniquely amenable to experimentation, which points to a key new line of experiments that could test many aspects of the mechanisms and potential functions of complex patterns.

Acknowledgments

a Keck Scholars Award (to B.G.C.); Grant sponsor: National Institutes of Health; Grant number: RO1 DA020942 (to B.G.C.); Grant sponsor: the University of Virginia Medical Scientist Training Program (to J.J.C.).

We thank all members of the Condron lab for helpful discussions. We also thank Yuan Yan Chen for his expertise in statistics. The 1D4 monoclonal antibody developed by A.H. Helt and C.S. Goodman was obtained from the Developmental Studies Hybridoma Bank developed under the auspices of the NICHD and maintained by The University of Iowa, Department of Biological Sciences, Iowa City, IA 52242.

LITERATURE CITED

Bartumeus F, Catalan J, Fulco UL, Lyra ML, Viswanathan GM. Optimizing the encounter rate in biological interactions: Levy versus Brownian strategies. Phys Rev Lett 2002;88:097901–097904. [PubMed: 11864054]

Bassingthwaighte, J.; Liebovitch, L.; West, B. American Physiological Society. New York: Oxford University Press; 1994. Fractal physiology.

Beggs JM, Plenz D. Neuronal avalanches in neocortical circuits. J Neurosci 2003;23:11167–11177. [PubMed: 14657176]

Bunin MA, Wightman RM. Quantitative evaluation of 5-hydroxy-tryptamine (serotonin) neuronal release and uptake: an investigation of extrasynaptic transmission. J Neurosci 1998;18:4854–4860. [PubMed: 9634551]

Bunin MA, Wightman RM. Paracrine neurotransmission in the CNS: involvement of 5-HT. Trends Neurosci 1999;22:377–382. [PubMed: 10441294]

Chazal G, Ralston HJ 3rd. Serotonin-containing structures in the nucleus raphe dorsalis of the cat: an ultrastructural analysis of dendrites, presynaptic dendrites, and axon terminals. J Comp Neurol 1987;259:317–329. [PubMed: 3294934]

Chen JC, Condron BG. Branch architecture of the fly larval abdominal serotonergic neurons. Dev Biol 2008;320:30–38. [PubMed: 18561908]

Condron BG. A freeware JAVA tool for spatial point analysis of neuronal structures. J Neuroinformatics 2008;6:57–61.

Daubert EA, Condron BG. A solid-phase immunostaining protocol for high-resolution imaging of delicate structures in the *Drosophila* larval central nervous system. CSH Protocols. 200710.0010/pbd.prot4771

De-Miguel FF, Trueta C. Synaptic and extrasynaptic secretion of serotonin. Cell Mol Neurobiol 2005;25:297–312. [PubMed: 16047543]

Diggle, PJ. Statistical analysis of spatial point patterns. London: Oxford University Press; 2001.

Edwards AM, Phillips RA, Watkins NW, Freeman MP, Murphy EJ, Afanasyev V, Buldyrev SV, da Luz MG, Raposo EP, Stanley HE, Viswanathan GM. Revisiting Levy flight search patterns of wandering albatrosses, bumblebees and deer. Nature 2007;449:1044–1048. [PubMed: 17960243]

Eguiluz VM, Chialvo DR, Cecchi GA, Baliki M, Apkarian AV. Scale-free brain functional networks. Phys Rev Lett 2005;94:018102-1–018102-4. [PubMed: 15698136]

Goldberger AL, Amaral LA, Hausdorff JM, Ivanov P, Peng CK, Stanley HE. Fractal dynamics in physiology: alterations with disease and aging. Proc Natl Acad Sci U S A 2002;99(suppl 1):2466–2472. [PubMed: 11875196]

Grenningloh G, Rehm EJ, Goodman CS. Genetic analysis of growth cone guidance in *Drosophila*: fasciclin II functions as a neuronal recognition molecule. Cell 1991;67:45–57. [PubMed: 1913818]

Helt, AH. PhD Thesis. University of California; Berkeley: 1997. Data visualization and gene discovery in *Drosophila melanogaster*.

Hughes ME, Bortnick R, Tsubouchi A, Baumer P, Kondo M, Uemura T, Schmucker D. Homophilic dscam interactions control complex dendrite morphogenesis. Neuron 2007;54:417–427. [PubMed: 17481395]

Jacobs BL, Azmitia EC. Structure and function of the brain serotonin system. Physiol Rev 1992;72:165–229. [PubMed: 1731370]

Mandelbrot, BB. Fractals: form, chance, and dimensions. San Francisco: W.H. Freeman & Company; 1977.

Mathew D, Popescu A, Budnik V. *Drosophila* Amphiphysin functions during synaptic fasciclin II membrane cycling. J Neurosci 2003;23:10710–10716. [PubMed: 14627656]

Matthews BJ, Kim ME, Flanagan JJ, Hattori D, Clemens JC, Zipursky SL, Grueber WB. Dendrite self-avoidance is controlled by dscam. Cell 2007;129:593–604. [PubMed: 17482551]

McNamee JE. Fractal perspectives in pulmonary physiology. J Appl Physiol 1991;71:1–8. [PubMed: 1917729]

Meinertzhagen IA, Govind CK, Stewart BA, Carter JM, Atwood HL. Regulated spacing of synapses and presynaptic active zones at larval neuromuscular junctions in different genotypes of the flies *Drosophila* and *Sarcophaga*. J Comp Neurol 1998;393:482–492. [PubMed: 9550153]

Moukhles H, Bosler O, Bolam JP, Vallee A, Umbriaco D, Geffard M, Doucet G. Quantitative and morphometric data indicate precise cellular interactions between serotonin terminals and postsynaptic targets in rat substantia nigra. Neuroscience 1997;76:1159–1171. [PubMed: 9027876]

Novotny T, Eiselt R, Urban J. Hunchback is required for the specification of the early sublineage of neuroblast 7-3 in the *Drosophila* central nervous system. Development 2002;129:1027–1036. [PubMed: 11861485]

Plenz D, Thiagarajan TC. The organizing principles of neuronal avalanches: cell assemblies in the cortex? Trends Neurosci 2007;30:101–110. [PubMed: 17275102]

Plotnick RE, Gardner RH, Hargrove WW, Prestegaard K, Perlmutter M. Lacunarity analysis: a general technique for the analysis of spatial patterns. Phys Rev E Statistical Physics Plasmas Fluids Relat Interdisciplinary Top 1996;53:5461–5468.

Rusakov DA, Kullmann DM, Stewart MG. Hippocampal synapses: do they talk to their neighbours? Trends Neurosci 1999;22:382–388. [PubMed: 10441295]

Soba P, Zhu S, Emoto K, Younger S, Yang SJ, Yu HH, Lee T, Jan LY, Jan YN. *Drosophila* sensory neurons require dscam for dendritic self-avoidance and proper dendritic field organization. Neuron 2007;54:403–416. [PubMed: 17481394]

Sykes PA, Condron BG. Development and sensitivity to serotonin of *Drosophila* serotonergic varicosities in the central nervous system. Dev Biol 2005;286:207–216. [PubMed: 16122730]

Vallés AM, White K. Development of serotonin-containing neurons in *Drosophila* mutants unable to synthesize serotonin. J Neurosci 1986;6:1482–1491. [PubMed: 3086515]

Viswanathan GM, Buldyrev SV, Havlin S, da Luz MG, Raposo EP, Stanley HE. Optimizing the success of random searches. Nature 1999;401:911–914. [PubMed: 10553906]

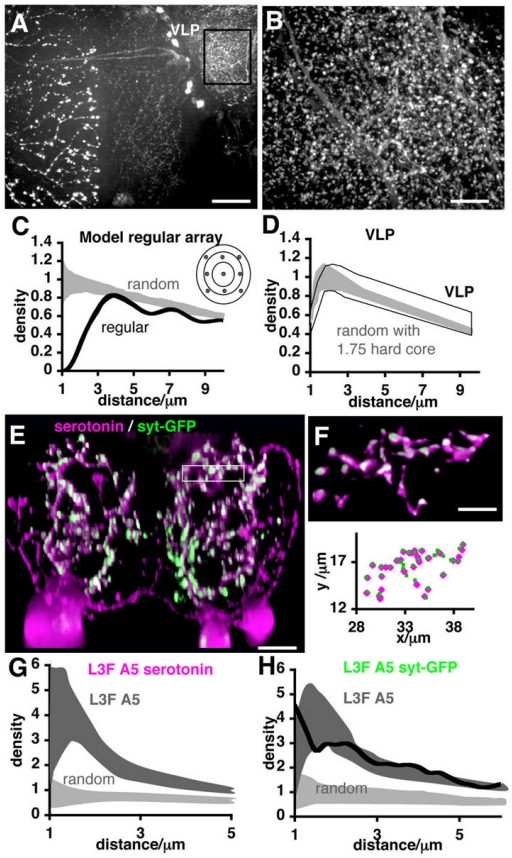

Figure 1.

Density distributions of serotonergic varicosities in various parts of the *Drosophila* CNS. **A:** Serotonin staining of an adult *Drosophila* left brain. The medulla is on the left, the lobula in the center, and the central brain on the right. The ventrolateral protocerebrum (VLP) of the central brain (square) has, by visual inspection, the highest varicosity density. **B:** Higher magnification image of the region indicated in A. Varicosity density is about twice that seen in most other CNS regions. **C:** The density distribution of varicosities is measured by normalizing the local density in a sphere around any varicosity to the bulk density. The sphere radius is increased in 0.25-μm steps starting at 1 μm. Shown are 99% confidence intervals of random (light gray) and regular (black) distributions. Both patterns were generated from a single VLP sample, but the points were moved to either random positions, or onto a 3-μm grid with some noise added. The drop-off in random density with increasing sample sphere radius is due to edge effects. The sinusoidal regular distribution is due to sample spheres intersecting points on the grid. **D:** Density distribution of VLP varicosities compared with a random pattern with a 1.75-μm hardcore (region of avoidance around each point). The VLP pattern (black) is very similar to a random distribution (C) except that there is a sharp drop-off in density below 1.75 μm. Using the random model in C and introducing a 1.75-μm hardcore avoidance produces a pattern very similar to the VLP (light gray). **E:** A single abdominal segment of a third-instar larval CNS stained for serotonin (cyan) and synaptic-localized GFP (green). **F:** Higher magnification of the boxed region in E has been rotated (top panel) and classified for the Cartesian coordinates of serotoninergic puncta (cyan, inset) and GFP puncta (green, inset). **G,H:** Density distribution of varicosities based on serotonin-puncta (dark gray, G) and syntaxin-GFP (dark gray, H). The plot shows the 99% confidence intervals, computed from six samples compared witho Monte Carlo simulated random samples (light gray). In both cases, the pattern is clustered over the entire span measured, with a slight peak around 1.75 μm as in

D. H: Plot of an average density distribution of varicosities, in black, from six branches in which only varicosities on other branches are included. This removes the density due to proximity of en passant varicosities. Scale bar = 40 μm in A; 10 μm in B,E,F.

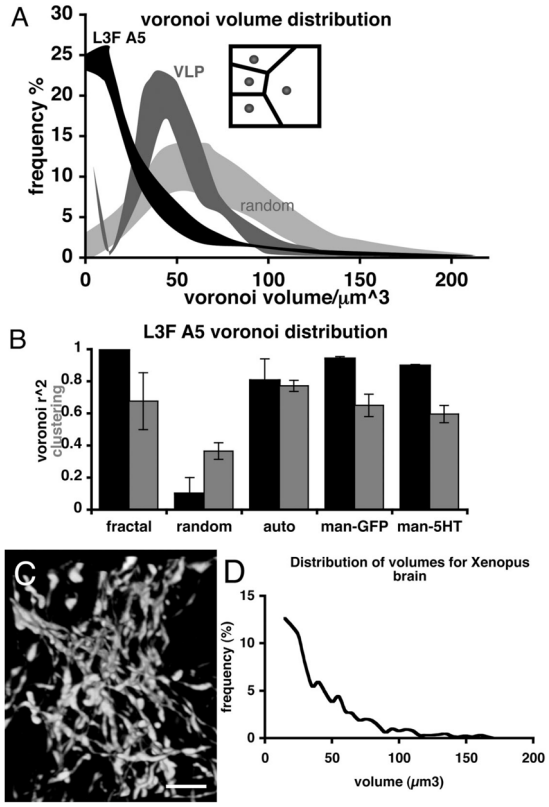

Figure 2.

Tessellation analysis reveals a clustered distribution of Voronoi volumes. **A:** A frequency distribution of Voronoi volumes surrounding varicosities indicates a clustered distribution for L3F A5 (black) compared with random(light gray). The ventrolateral protocerebrum(VLP) distribution has a sharper peak than that of random, indicating some regularity (dark gray). The distribution of serotonergic varicosities in L3F A5 is significantly different from the distribution seen in VLP and a random pattern (Kolmogorov Smirnov test; $P < 0.0001$). With the exception of volumes less than 10μm^3, L3F A5 has a smooth distribution that linearizes on a log-log plot (Fig. 3C). **B:** Voronoi distributions were analyzed by either linear fit on a log-log plot (r^2, black bars) or degree of clustering (coefficient of variation, gray bars). Different methods were used to test data collection and tessellation algorithms on the L3F A5 distribution. In each case, six samples were used and the 99% confidence intervals shown. For comparison, fractal and random distributions are also shown. The L3F A5 data set has an r^2 value significantly higher than both random and regular distributions (Fisher z transformation; $P < 0.001$). PAJ refers to the software package used to determine the Voronoi distributions, which was used in all cases except when a Matlab algorithm was also utilized for confirmation of the PAJ analysis. Serotonergic varicosities were scored either automatically (Auto) by using the Improvision Volocity classifier or manually (man) and identified by either serotonin staining or synaptic-directed GFP. Clustering is the same for all L3F A5 data sets and is the same as a fractal pattern. The r^2 value for manually collected varicosities is higher than that for auto-classified data. **C:** Serotonin staining of a *Xenopus* tadpole diencephalon. **D:** Voronoi volume distribution of *Xenopus* data. 5HT, serotonin. Scale bar = 10 μm in C.

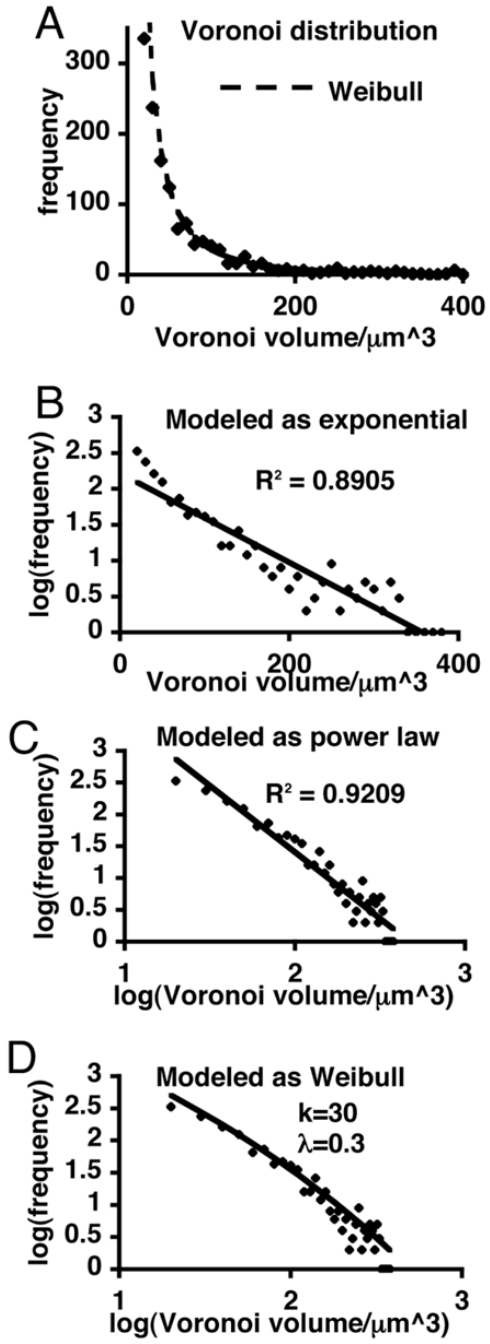

Figure 3.

Voronoi volume distribution. **A:** To analyze the distribution of Voronoi volumes, 1,601 measures, ranging from 1 to 954 μm^3 from six samples of L3F A5 are plotted as a frequency distribution. The dashed line represents an ideal Weibull distribution. **B,C:** The data from A were then transformed into either (B) log-(frequency), or (C) log-(frequency) versus log-(volume). The plots were linear fitted and the least-squares r^2 measure indicated. The distribution fits a log-log power law ($r^2 = 0.9209$) better than a log-normal ($r^2 = 0.8905$). **D:** The data in C are now plotted but fitted to a Weibull distribution ($k = 30$, $\lambda = 0.3$) that best fits the data by visual inspection.

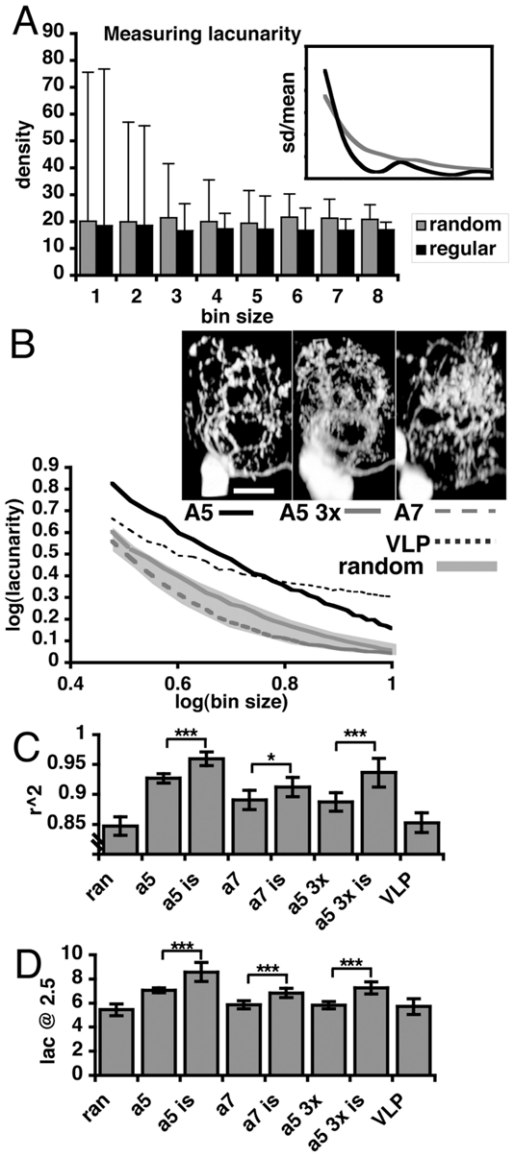

Figure 4.

Lacunarity analysis indicates clustered distribution of varicosities. **A:** Lacunarity is a measure of how sample variance changes with sample size. Plotted is the average density of a 3D point distribution versus an increasing sample cube vertex size for a random (gray) and regular (black) distribution (4-μm grid). The standard deviation decreases smoothly for the random distribution, whereas the regular pattern has peaks corresponding to the regular 4-μm grid on which the points are arrayed. Lacunarity is calculated as (1 + variance)/mean^2. Inset is a log/log plot of coefficient of variation versus sample size showing the peaks on the regular pattern versus the smooth curve of the random pattern. **B:** Log-log plot of the lacunarity analyses of single samples of VLP, A5 segment, triplicated A5 (A5 3×, overexpression of Hb protein), A7 segment compared with a random pattern (gray). Both A5 3× and A7 curves lie within the random intervals, whereas the ventrolateral protocerebrum (VLP) curve lies above the random interval, indicating it is more clustered than random. The A5 curve also lies above the random interval and is more linear than the other distributions, which is quantified by r^2 in C. **C,D:** The log-log plot of lacunarity values in C is quantified by either the r^2 (C) for the fit to a

straight line on a log-log plot, or clustering by the height of the lacunarity curve at 2.5 μm (lac @ 2.5; D). All values are averages with 99% confidence intervals either computed for six data samples or, in the case of random (ran), determined by 100 randomized models. In each case, varicosity distributions were analyzed either for segments with contributions from adjacent cells, or for those segments in which all neighboring neurons were ablated (Chen and Condron, 2008). Isolating cells significantly increases the clustering of the distribution. *, $P < 0.05$; **, $P < 0.01$; ***, $P < 0.001$ by Student's t-test. Scale bar = 20 μm in B.

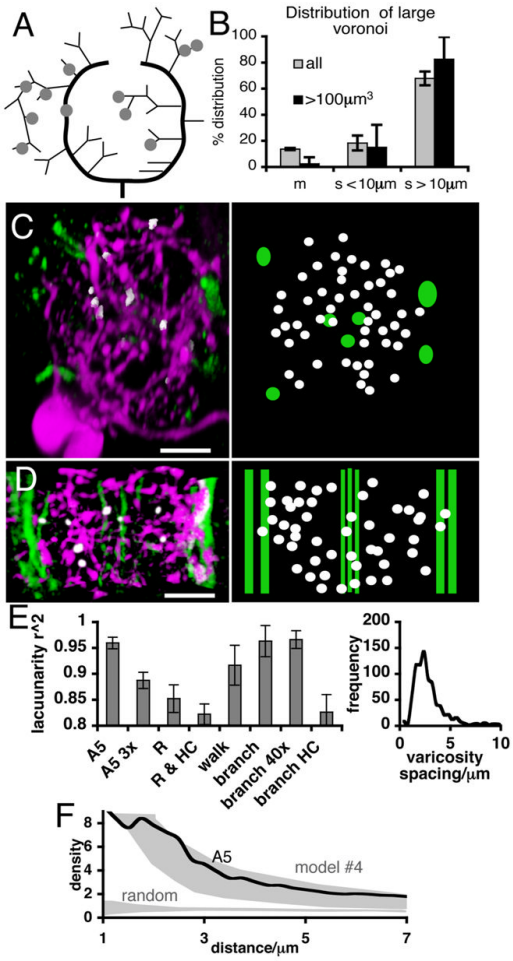

Figure 5.

Clusters are not specifically localized and model as a random branched structure. **A,B:** To see whether varicosities with large surrounding spaces (Voronoi volumes) are topologically organized, those with volumes > 100 μm^3 were marked on reconstructed dendrograms. These patterns were then examined over six reconstructed medial cell samples, and positions on the tree were marked as m, for main branch, s < 10 μm, for those varicosities within the first 10 μm of secondary branches and s > 10 μm for the more distal parts of varicosities. The positions of all volume > 100 μm^3 varicosities are shown for one dendrogram (A). B: Percentage distribution of varicosities on the dendrogram for six samples either for all varicosities or for those with large Voronoi volumes. **C,D:** Varicosities with >100 μm^3 Voronoi volumes were marked on actual samples (white/cyan, serotonin; green, fasciclin II) and their relative neuropil positions were noted by using fasII-stained axon bundles as a fiduciary marker. C: Shown at left is one actual sample and at right an overlay of six samples, using fasII as reference points. The view is of one cropped A5 left hemisegment with dorsal at top. D: The same data rotated 90° with anterior at the top. In each case, the midline is on the right. Again, shown at left is one actual sample and at right an overlay of six samples. No pattern or distinct localization of varicosities with >100 μm^3 Voronoi volumes is apparent. **E:** Lacunarity of data samples was compared with a number of computer models. Two measures were taken for each lacunarity curve, r^2 and lac@2.5 as in Figure 4. Error bars are 99% confidence intervals and were computed for A5 and A5 3×, and determined from 100 simulations for each of the models. R, random model; R & HC, random with a 1.75-μm hardcore avoidance; walk, a single wandering branch where varicosities are spaced linearly apart according to L3F (distribution in right

panel); branch, same as walk except that 1/5 varicosities randomly form side branches; branch 40×, same as branch except 40 independent overlapping branched structures form; branch HC, same as branch except with a 1.75-μm hardcore avoidance. The branch model produces lacunarity measures that are very similar to the data. Avoidance (branch HC) but not increased number of branches (branch 40×) significantly degrades the similarity to data. The 2D spaces between varicosities along branches for 835 L3F A5 varicosities are measured and plotted as a frequency distribution (right panel). The distribution is left shifted normal with ranges from 0.14 to 17.4 μm. **F:** The density distribution of model 4 (upper gray) is, except for the smallest scales, very similar to data plot of single A5. Scale bar = 10 μm in C,D.

TABLE 1

Fitting to a Power Law[1]

	linear regression, μ	MLE for μ	MLE for λ	AIC power law	AIC exponential
L3W (20–330)	1.845	1.83	0.156	0.1	0.9
fractal (20–2000)	1.816	1.845	0.0095	1	2.445E–46
fractal (20–290)	1.874	2.076	0.02125	0.45	0.55
Lobula (20–120)	2.92	3.08			
random (100–210)	3.05	4.43			

[1]Linear regression is calculated from the slope of the log-log Voronoi plot. The maximum likelihood estimation (MLE) for μ and the MLE for λ are calculated from the equations provided in Edwards et al. (2007). These were calculated within the bounded ranges that encompass the peak through the tail of the Voronoi volumes for each of the distributions (shown in parentheses). The μ for the A5 segment calculated by linear regression and MLE is consistent with a power law distribution ($1 < \mu \leq 3$). However, the Akaike weights for A5 favor an exponential distribution (0.90) over a power law distribution (0.10). Idealized fractal data sets are also shown, with one that is bounded from 20 to 2,000 and the other from 20 to 290. Both fractal data sets have μ consistent with a power law distribution. Truncating the tail of an idealized fractal data set results in Akaike weights that favor an exponential over a power law distribution. The μ calculated by linear regression and MLE for a random data set and lobula are also shown.